Morphology Development and Non-Isothermal Crystallization Behavior of Polyamide 11/Ethylene-vinyl Alcohol Blends

Yingchun Li, Guosheng Hu, Biaobing Wang

Institute of Macromolecules and Bioengineering, North University of China, Taiyuan 030051, China

Received 21 December 2009; accepted 22 March 2010
DOI 10.1002/app.32495
Published online 11 June 2010 in Wiley InterScience (www.interscience.wiley.com).

ABSTRACT: High-barrier polyamide 11 (PA11) was prepared by *in situ* co-crosslinking technology using ethylene-vinyl alcohol (EVOH) as the barrier layer, and the morphology development and non-isothermal crystallization behavior were investigated. The scanning electron microscope (SEM) observations demonstrated that the morphology development was greatly dependent on the concentration of dicumyl peroxide (DCP). A pronounced lamellar morphology was obtained at 1.5% DCP loading level. The analysis of non-isothermal crystallization kinetics indicated that the addition of EVOH and DCP affected the crystallization mode of PA 11. Notably, the crystallization rate of PA 11 was related with the morphology of EVOH and the interaction between EVOH and PA 11. © 2010 Wiley Periodicals, Inc. J Appl Polym Sci 118: 2126–2133, 2010

Key words: polyamide 11; ethylene-vinyl alcohol; laminar morphology; barrier property; non-isothermal crystallization kinetics

INTRODUCTION

In recent years, PA 11 is one of the most promising engineering plastics for several reasons, one of which is that its starting material is from renewable castor oil. In addition, its major application is used for automobile pipe-laying and municipal gas pipe as well as offshore oilfield applications due to its high self-lubricating property and oil-barrier properties. However, it is important to note that the barrier properties of the neat PA 11 resin can not meet with the strict regulations of environmental protection. In addressing the issue of barrier-improvement, there are still many works to be done. Ethylene-vinyl alcohol copolymer (EVOH) is often recognized as a barrier material due to its superior gas barrier properties and high oil resistance.[1–3] Some literatures have reported on the investigation of the barrier properties of polyamide (PA)/ EVOH and/or modified PA (MPA)/EVOH blends over the past few years.[4–10]

The final properties of polymer/polymer blends are usually controlled by the properties of the components, morphology of the blends, and interaction between components in the blends.[11–13] In the immiscible blends, the phase morphology determines, to a large extent, the permeability of the blends. Numerous investigations have demonstrated that the multilamellar morphology is influenced by the following factors: the concentration of the dispersed phase,[14–16] processing conditions,[17–20] melt shear viscosity ratio of the dispersed phase to the continuous phase,[21–25] etc. Moreover, the morphology and the interaction between the components have great influence on the primary effects of crystallization, for example, the nucleation and growth rate, which in turn affect the physical, chemical, and mechanical properties of crystalline polymer.

EVOH copolymers do not have a good compatibility, adhesion, or miscibility with other polymers whether of polar or non-polar nature since EVOH copolymers are strongly self-associated. The interassociation of the hydroxyl groups of EVOH with, for instance, the carbonyl groups of complementary polymers is comparatively weak.[26] Miscibility of EVOH copolymer with PA has been studied by several authors. Specific interaction between EVOH and PA was observed, resulting in partial miscibility of the components.[27–29] Despite of partial miscibility, blending of EVOH into PA had also been demonstrated to deteriorate the mechanical properties of the PA matrix.[30,31]

Therefore, the overall focus of our work is to improve the barrier properties while not to sacrifice other properties of the PA 11 matrix. Taking these

Correspondence to: B. Wang (bbwang@nuc.edu.cn).
Contract grant sponsor: Science and Technology Foundation for Youth (Shanxi Sci and Tech Bureau); contract grant number: 2006021011.

issues into consideration, we developed a new *in situ* co-crosslinking technology to prepare high-barrier PA 11/EVOH blend. Our previous work[32] confirmed the co-crosslinking between PA 11 and EVOH in the presence of dicumyl peroxide (DCP), which was contributed to the improvement of mechanical properties of the blends. The effect of the DCP loading level on the melting behavior and isothermal crystallization kinetics of PA 11/EVOH/DCP ternary blends were also discussed in another publication.[33]

The purpose of this study is to investigate the morphology development and non-isothermal crystallization kinetics. The morphology development with the varying DCP concentration is observed by scanning electron microscope (SEM). Differential scanning calorimetry (DSC) was adopted to characterize the crystalline nature of PA 11 in the blends, and analyze the non-isothermal crystallization kinetics by the Jeziorny equation and the Mo method.

EXPERIMENTAL SECTION

Materials

PA 11 was prepared according to the synthesis procedure reported in the literature,[33] its weight-average ($\overline{M}_w$) and number-average ($\overline{M}_n$) molecular weights are 19.8 $\times$ 104 g/mol and 4.0 $\times$ 104 g/mol, respectively. The EVOH (F101B) was obtained from Kuraray (Japan), ethylene content, 32 mol %. DCP was supplied by Gaoqiao Petrochemical Corporation (Shanghai, China).

Preparation of blends

PA 11 and EVOH were dried under vacuum at 80°C for 12 h and kept in desiccator before use. Melt blends were obtained by using a SJ20/25 single-screw extruder (China). The screw speed was 70 rpm, and the temperature of the feed, middle, and extruded regions were 190°C, 220°C, and 220°C, respectively. The extrudate was passed through a cooling water bath, pelletized, and dried under vacuum at 80°C for 24 h.

In this article, the PA 11/EVOH (PA 11/EVOH = 80/20) blends containing 0% DCP and X% DCP were abbreviated as NED-0 and NED-X, respectively.

Scanning electron microscopy

The electron microscope (Hitachi S530) was used to examine the morphology of the blends. The fractured surface was previously treated for 24 h with a boiling dioxane–water mixture and then coated with a thin layer of gold. Such dioxane–water mixture is a strong solvent for EVOH, whereas it is ineffective on PA 11. Therefore, it is possible that EVOH phase is selectively etched by the mixture. The remaining holes reflect the distribution of the dispersed EVOH domains in the PA 11 matrix.

Differential scanning calorimetry analysis

Non-isothermal crystallization process was carried out using a Mettler DSC822[e] and the temperature was calibrated with the indium standard. All DSC experiments were performed under a nitrogen purge at a constant flow rate. Sample weight was between 2 and 3 mg. All samples were dried at 80°C under vacuum for 12 h before measurement.

In the non-isothermal crystallization process, the sample was first heated to 230°C at a heating rate of 20°C/min and held for 10 min to eliminate any previous thermal history, and then cooled at rates of 2.5, 5, 10, 20, and 40°C/min. The exothermal curves of heat flow as a function of temperature were recorded to analyze the non-isothermal crystallization process of the neat PA 11 and its blends.

RESULTS AND DISCUSSION

Morphology development

Many investigations on the multilamellar morphology have demonstrated that the number and size of layers are largely dependent on the concentration of the dispersed phases. However, under the constant concentration of the dispersed phases, the multilamellar morphology is controlled by the viscosity ratio of the two phases, the level of the interfacial adhesion and the processing method. Moreover, as required for lamellar morphology, the viscosity ratio between the dispersed phase and the matrix should be a value greater than 1. As the PA 11 matrix has a higher viscosity than the EVOH, it can transfer the shear force more easily onto the softer EVOH phase, a fine EVOH phase dispersion can be obtained. Therefore, the DCP as a cross-linking agent was incorporated into the PA 11/EVOH blends to enhance the viscosity of EVOH through the co-crosslinking between EVOH and PA 11, which was supposed to contribute to the lamellar morphology development.

The effect of DCP concentration on the morphology of PA 11/EVOH/DCP blends was investigated using SEM (Fig. 1). As shown in Figure 1(a), a clear phase separation occurred in the PA 11/EVOH binary blend at a weight ratio of 80/20. When 0.5% DCP was incorporated into the PA 11/EVOH blend, more fine spherical domains and no lamellar layers were found, as shown in Figure 1(b). Some lamellar

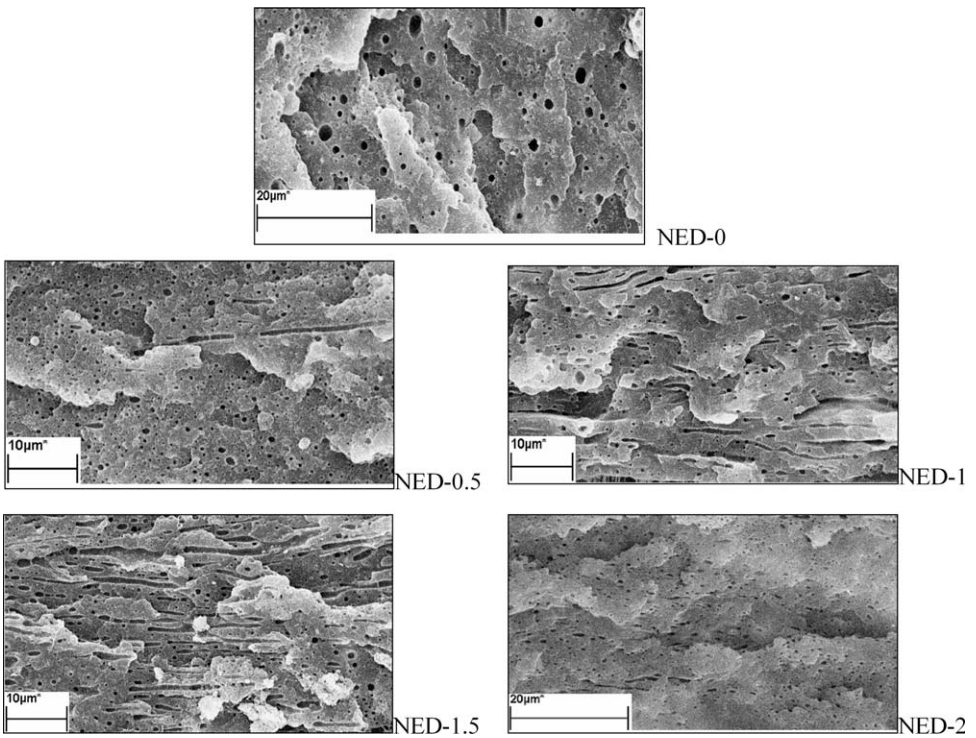

Figure 1 SEM micrographs of PA 11/EVOH/DCP blends with various DCP concentration. (a) 0; (b) 0.5%; (c) 1%; (d) 1.5%; and (e) 2%.

structures occurred with further increasing DCP concentration. A large number of thinner and longer layers of EVOH were obtained in the case of 1.5% DCP [Fig. 1(d)]. That is, a pronounced lamellar morphology was developed in this case. However, only few thicker and shorter layers and more spherical domains were formed at 2% loading level of DCP, as shown in Figure 1(e). It was speculated that the morphology development may correlate with the co-crosslinking reaction between the dispersed EVOH phases and the PA 11 matrix. It was speculated that the viscosity of the EVOH, although was improved by the co-crosslinking reaction, was still lower than that of the PA 11 at lower DCP loading level. Hence, the PA 11 matrix can transfer more readily the shear stress onto the EVOH. In the case of the medium value of DCP, partial EVOH melts were strong enough to stretch their domains into the elongated laminas during the extrusion process. As such, a partial lamellar structure was generated [Fig. 1(c)]. The optimum DCP concentration makes the melt strength of the EVOH not too hard or too soft, so it favors the formation of a well-developed laminar morphology. However, when the DCP content was increased to 2% in our system, the viscosity of the cross-linked EVOH was high enough to yield larger deformed domains before extrusion and was an unfavorable condition for extending the EVOH domains.

Non-isothermal crystallization kinetics

Figure 2 presented the non-isothermal crystallization curves for all specimens at various cooling rates. Clearly, the crystallization peak became broader and the crystallization peak temperature (Table I), T_p, which corresponds to the maximum crystallization rate, shifted gradually to low temperature with the increase of the cooling rates.

The relative crystallinity, $X_c(T)$, as a function of temperature, can be defined as follows[34]:

$$X_c(T) = \frac{\int_{T_0}^{T} \frac{dH_c(T)}{dT} dT}{\int_{T_0}^{T\infty} \frac{dH_c(T)}{dT} dT} \quad (1)$$

where T_0 and T_∞ are the initial and final crystallization temperature, respectively. In the non-isothermal crystallization process, time t has the relation with temperature T as follows:

$$t = \frac{|T_0 - T|}{\phi} \quad (2)$$

where T is the temperature at time t, and ϕ is the cooling rate.

Figure 3(a,b) depicted the typical plots of $X(T) \sim T$ and $X(t) \sim t$ for NED-1 sample, respectively. The initial crystallization temperature decreased as

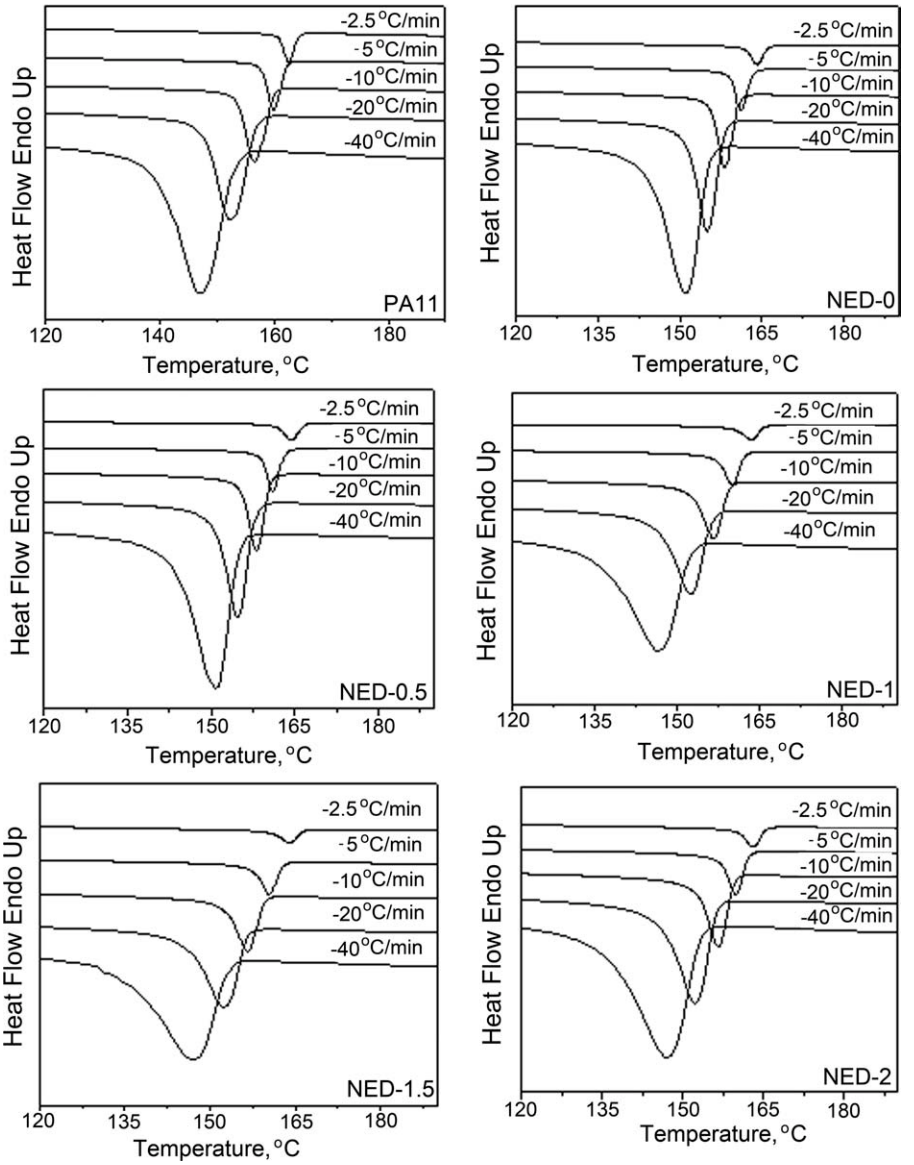

Figure 2 Non-isothermal crystallization curves of the neat PA 11 and its blends.

the cooling rate increased, indicating that there is no enough time to activate the nuclei at higher temperature when crystallized at higher cooling rate. In addition, the time required to reach the maximum crystallization rate, t_{max}, for the PA 11/EVOH blend was greater than that for the pure PA 11 at a specific cooling rate, suggesting the incorporation of EVOH hindered the crystallization process of PA 11. The much prolonged t_{max} values for the PA 11/EVOH/DCP ternary blends inferred that the addition of DCP further restricted the mobility of PA 11 chains.

On the basis of the assumption that the crystallization temperature is constant, non-isothermal crystallization can be described by the Avrami equation[35,36]

$$1 - X(t) = \exp[-Z_t t^n]$$

or

$$\lg\{-\ln[1 - X(t)]\} = n \lg t + \lg Z_t \quad (3)$$

where $X(t)$ is the relative degree of crystallinity, n is the Avrami exponent, t is the time, and Z_t is the overall crystallization rate constant. Considering the non-isothermal character of the process investigated, Jeziorny[37] suggested that the parameter, Z_t, should be corrected as follows:

$$\lg Z_c = \frac{\lg Z_t}{\phi} \quad (4)$$

All curves in the plots of $\lg(-\ln(1 - X(t)))$ versus $\lg t$ for NED-1.5 sample (Fig. 4) can be divided into

TABLE I
Some Parameters Determined from Non-Isothermal Crystallization Curves

Sample	ϕ (°C/min)	T_p (°C)	t_{max} (min)	ΔH_c (J/g)
PA 11	2.5	162.73	1.378	45.82
	5	160.27	0.905	52.57
	10	157.03	0.596	56.04
	20	152.84	0.384	56.80
	40	147.37	0.271	55.90
NED-0	2.5	164.28	2.422	41.09
	5	161.50	1.218	44.18
	10	158.71	0.606	46.99
	20	155.52	0.355	48.60
	40	151.99	0.214	48.72
NED-0.5	2.5	164.50	2.822	49.81
	5	161.31	1.299	51.95
	10	158.53	0.680	53.87
	20	155.54	0.353	54.34
	40	151.41	0.190	53.87
NED-1	2.5	163.64	2.679	50.57
	5	160.26	1.254	52.13
	10	157.10	0.652	52.57
	20	153.37	0.389	52.07
	40	147.76	0.251	49.89
NED-1.5	2.5	164.12	2.619	41.74
	5	160.61	1.255	45.46
	10	156.79	0.580	48.87
	20	152.72	0.355	50.13
	40	147.84	0.214	48.8
NED-2	2.5	163.17	2.439	61.37
	5	160.05	1.159	67.18
	10	156.99	0.624	70.40
	20	152.79	0.399	71.58
	40	147.94	0.245	70.37

two linear sections: the primary crystallization stage and the secondary crystallization stage. The values of n and Z_t (Table II) can be determined from slope and intercept of the fitted lines, respectively. At the primary crystallization stage, the various values of n_1 for the pure PA 11 (4.26–5.08) and the PA 11/EVOH blends (3.54–6.34) indicated that the incorporation of EVOH and DCP affected the primary crystallization mode of PA 11. At the second stage, the spherulites' growth transforms into a mixture mode of one- and two-dimensional space extension, as revealed by the n_2 values (1.157–1.933 for the pure PA 11 and 1.044–1.973 for its blends). On the other hand, the Z_{c2} value for the blends at a specific cooling rate (except 2.5°C/min) was almost the same as that of the pure PA 11, suggesting that the addition of EVOH and DCP had very little influence on the secondary crystallization rate of PA 11.

The modified crystallization rate parameters at the primary crystallization stage were more complicated and depended on the cooling rate and the DCP concentration. As compared with that of the pure PA 11, the Z_{c1} values of the PA 11/EVOH binary blends decreased at lower cooling rate ($\phi \leq$ 5°C/min) but increase at higher cooling rate ($\geq$10°C/min). When 0.5% DCP was added into the PA 11/EVOH blend, the Z_{c1} value reduced at whole range of the cooling rates; thereafter, it increased at $\phi \leq$ 5°C/min while decreasing at $\phi \geq$ 10°C/min with the increasing DCP loading level. Such behaviors can be interpreted from the crystallization kinetics of polymers. Generally, the crystallization kinetics of polymers is a complicated process that involves two important steps, that is, nucleation and crystal growth. As the diffusive molecule reaches the crystal boundary, it must form a stable nucleus, and it is followed by the growth of the crystallites. Thus, the process steps are affected, to a certain degree, by the thermodynamic conditions in which the crystallization takes place, by the molecular characteristics, and by the interaction between polymer and filler. In the non-isothermal crystallization process, the crystallization rate when crystallized at a higher cooling rate is controlled by the nucleation since there is no enough time to nucleate at higher temperature. Inversely, it is controlled by the crystal growth at a lower cooling rate. The folding of PA 11 chains into the nucleus surface was restricted by the chemical

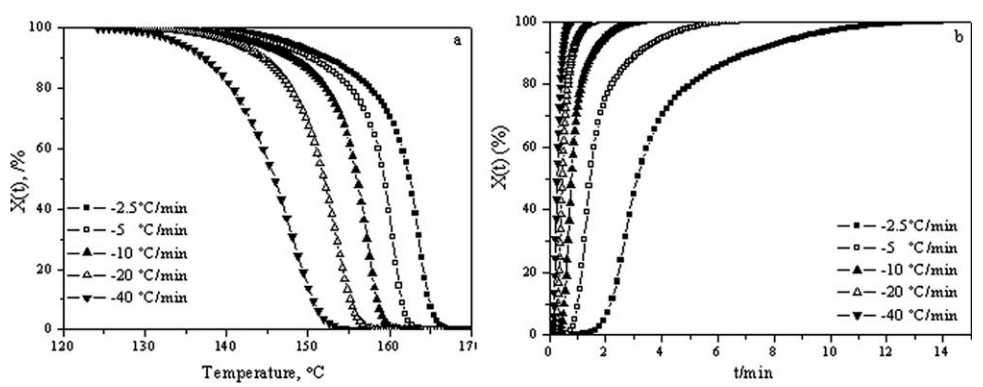

Figure 3 A typical plot of (a) $X(T) \sim T$ and (b) $X(t) \sim t$ for NED-1 sample at various cooling rate.

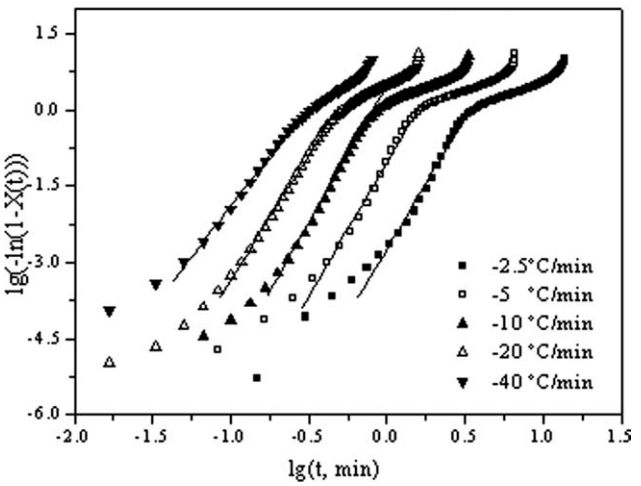

Figure 4 A typical plot of lg(−ln(1 − $X(T)$)) versus lg$t$ for NED-1 sample.

reaction between the hydroxide groups of EVOH and the carboxyl terminal groups of PA 11, leading to a slow crystallization rate at $\phi \leq 5$°C/min. The interaction further increased after the addition of DCP due to the formation of co-crosslinkages between the PA 11 and the EVOH, resulting in more serious hindrance of the mobility of the PA 11 chains. However, the β-scission of PA 11 chains predominates over the interaction between the PA 11 and the EVOH at high DCP concentration, the numerous broken PA 11 chain thus can readily fold into the nucleus surface and promote the crystal growth. It is also well known that a heterogeneous nucleation path makes use of a foreign preexisting surface to reduce the free energy opposing primary nucleation. The existence of the dispersed EVOH can create new surface [Fig. 1(a)] for the heterogeneous nucleation of the PA 11, leading to a fast crystallization at high cooling rate. On the other hand, the increased interactions after the addition of DCP limited the diffusion of the PA 11 chains to the crystal front and nucleation, resulting in a slow crystallization process. Therefore, at low DCP loading (e.g., NED-0 and NED-0.5 sample), the promotion by the preexisting surface of EVOH is predominant, the crystallization rate at $\phi \geq 10$°C/min increased as compared with that of the pure PA 11. Conversely, the crystallization rate at high DCP

TABLE II
Parameters Calculated from the Jezirony Equation

		Primary crystallization stage			Secondary crystallization stage		
Sample	ϕ (°C/min)	n_1	Z_{t1}	Z_{c1}	n_2	Z_{t2}	Z_{c2}
PA 11	2.5	4.272	0.112	0.416	1.572	0.701	0.868
	5	4.786	0.601	0.903	1.157	1.315	1.056
	10	5.080	5.702	1.190	1.209	1.977	1.071
	20	4.521	35.075	1.195	1.344	4.046	1.073
	40	4.258	153.11	1.134	1.993	11.749	1.064
NED-0	2.5	5.378	0.0039	0.109	1.550	0.285	0.605
	5	5.579	0.195	0.721	1.325	0.937	0.987
	10	5.458	6.299	1.201	1.151	2.057	1.075
	20	5.056	99.367	1.259	1.229	3.984	1.072
	40	4.814	650.830	1.176	1.611	9.400	1.058
NED-0.5	2.5	5.564	8.57×10^{-4}	0.0593	1.230	0.237	0.562
	5	6.336	0.0766	0.598	1.044	0.749	0.944
	10	6.263	3.688	1.139	1.026	1.476	1.040
	20	4.908	57.906	1.225	1.164	3.120	1.059
	40	4.379	322.65	1.154	1.527	7.835	1.053
NED-0-1	2.5	5.100	1.86×10^{-3}	0.0809	1.260	0.199	0.524
	5	5.290	0.0925	0.621	1.117	0.635	0.913
	10	5.387	2.819	1.109	1.226	1.344	1.030
	20	4.935	38.008	1.199	1.539	3.099	1.058
	40	3.950	113.671	1.126	1.879	10.689	1.061
NED-1.5	2.5	5.265	2.31×10^{-3}	0.0882	1.579	0.173	0.496
	5	5.545	0.143	0.678	1.356	0.667	0.922
	10	4.742	5.084	1.177	1.381	1.551	1.045
	20	4.369	27.73	1.181	1.530	3.150	1.059
	40	3.538	64.796	1.110	1.973	10.213	1.060
NED-2	2.5	4.952	4.8×10^{-3}	0.118	1.459	0.213	0.539
	5	5.053	0.151	0.685	1.196	0.670	0.923
	10	5.076	3.502	1.134	1.214	1.326	1.029
	20	5.127	35.831	1.196	1.422	2.577	1.0484
	40	3.930	86.964	1.118	1.839	6.576	1.0482

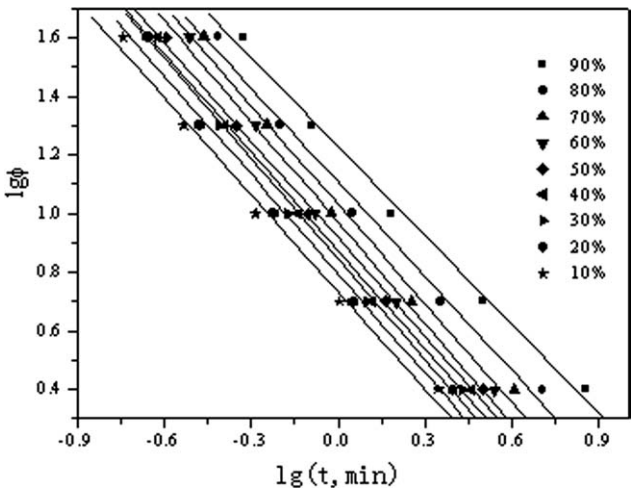

Figure 5 A typical plot of lgϕ versus lg*t* for NED-1 sample.

loading (≥1.0%) decreased since the hindrance surpassed the promotion.

To find a method to describe exactly the non-isothermal crystallization process, Mo and coworkers[38] have developed a novel kinetic approach by combining the Avrami equation [eq. (4)] with the Ozawa equation ($\lg\{-\ln[1 - X(T)]\} = \lg K(T) - m\lg\phi$),[39] the following equations are obtained at a given degree of crystallinity,

$$\lg Z_t + n\lg t = \lg K(T) - m\lg\phi$$

$$\lg\phi = \frac{1}{m}\lg\left[\frac{K(T)}{Z_t}\right] - \frac{n}{m}\lg t$$

$$\lg\phi = \lg F(T) - \alpha\lg t \quad (5)$$

where *K(T)* is the cooling function related to the overall crystallization rate, *m* is the Ozawa exponent, $F(T) = [K(t)/Z_t]^{1/m}$ is the value of cooling rate, which has to be chosen at a unit crystallization time when the measured system amounts to a certain degree of crystallinity, and $\alpha = n/m$. Plots of lgϕ versus lg*t* at a given degree of crystallinity were obtained according to eq. (7) and all curves exhibit good linear relationship (Fig. 5), revealing that the Mo model provides a satisfactory description to the non-isothermal crystallization for both the pure PA 11 and its blends. The values of α and *F(T)* (Table III) can be calculated from the slope and intercept of these lines, respectively. The *F(T)* values increased with the increasing relative degree of crystallinity, indicating that a higher cooling rate should be adopted to obtain a higher degree of crystallinity at unit crystallization time. Moreover, at a specific degree of crystallinity, the *F(T)* values for all the blends with or without DCP were greater than that for the pure PA 11. That is, approaching to an identical degree of crystallinity, the blends required higher cooling rate than that of the pure PA 11. In addition, the range of α values was 1.518–1.705 for the pure PA 11 and 1.014–1.314 for the blends, inferring that the addition of EVOH and DCP affected the crystallization mode of PA 11. This result was in agreement with that demonstrated by the Jeziorny method.

CONCLUSION

We evaluated the effect of DCP on the morphology develop of the EVOH within the PA 11 matrix in this study. SEM observations showed that the blends displayed different morphology (e.g., spherical and laminar domain), depending on the DCP loading level. Numerous thinner and longer layers of EVOH were obtained at 1.5% DCP concentration. The overall crystallization rate constant at the primary crystallization stage, which was obtained from the analysis of the Jeziorny equation, indicated that the non-isothermal crystallization process was related with the morphology development and the interaction between PA 11 and EVOH.

TABLE III
Parameters Calculated from the Mo Method

Sample	*X* (*t*)	10%	20%	30%	40%	50%	60%	70%	80%	90%
PA 11	*a*	1.518	1.581	1.601	1.638	1.639	1.663	1.679	1.703	1.705
	F(*T*)	2.793	3.373	3.926	4.395	4.977	5.559	6.194	7.362	9.931
NED-0	*a*	1.073	1.114	1.131	1.167	1.176	1.183	1.215	1.223	1.238
	F(*T*)	4.724	5.341	5.836	6.288	6.770	7.269	7.906	8.958	12.069
NED-0.5	*a*	1.014	1.018	1.021	1.048	1.046	1.069	1.088	1.076	1.026
	F(*T*)	5.521	6.235	6.711	7.265	7.723	8.431	9.536	11.585	15.907
NED-1	*a*	1.103	1.129	1.143	1.121	1.111	1.150	1.128	1.071	1.012
	F(*T*)	5.542	6.209	6.994	7.431	8.217	9.311	10.711	12.776	16.855
NED-1.5	*a*	1.184	1.193	1.201	1.179	1.167	1.177	1.212	1.112	1.027
	F(*T*)	4.852	5.608	6.341	6.951	7.643	8.545	9.821	11.796	15.577
NED-2	*a*	1.137	1.235	1.283	1.259	1.296	1.314	1.293	1.255	1.235
	F(*T*)	4.775	5.664	6.419	6.999	7.929	9.022	10.303	13.076	18.277

Reference

1. Lagarón, J. M.; Powell, A. K.; Bonner, J. G. Polym Test 2001, 20, 569.
2. Karos, W. J. Barrier Polymers and Structures; American Chemical Society: Washington, DC, 1989; 423.
3. Finch, C. A. Polyvinyl Alcohol; John Wiley and Sons: New York, 1992.
4. Takashige, M.; Kanai, T. Int Polym Process 2006, 21, 86.
5. Foldes, E.; Pukanszky, B. J Colloid Interface Sci 2005, 283, 79.
6. Lagaron, J. M.; Gimenez, E.; Gavara, R.; Saura, J. J. Polymer 2001, 42, 9531.
7. Lagaron, J. M.; Gimenez, E.; Saura, J. J.; Gavara, R. Polymer 2001, 42, 7381.
8. Cerruti, P.; Laurienzo, P.; Malinconico, M.; Carfagna, C. J Polym Sci Polym Phys 2007, 45, 840.
9. Yeh, J. T.; Yao, W. H.; Du, Q. G.; Chen, C. C. J Polym Sci Polym Phys 2005, 43, 511.
10. Incarnato, L.; Acierno, D.; Russo, P.; Mallinconico, M.; Laurienzo, P. J Polym Sci Polym Phys 1999, 37, 2445.
11. Hietaoja, B. D.; Holsti-Miethinen, J. P.; Ikkala, O. T. J Appl Polym Sci 1994, 54, 1613.
12. Wu, S. Polym Eng Sci 1987, 27, 3359.
13. Utracki, L. A.; Shi, Z. H. Polym Eng Sci 1992, 32, 1824.
14. Yeh, J. T.; Fanchiang, C. C.; Yang, S. S. J Appl Polym Sci 1997, 64, 1531.
15. Cui, X. G.; Wang, X. D. J Appl Polym Sci 2006, 101, 3791.
16. Lee, S. Y.; Kim, S. C. J Appl Polym Sci 1998, 67, 2001.
17. Huang, H. X.; Huang, Y. F.; Yang, S. L. Polym Int 2005, 54, 65.
18. Garmabi, H.; Kamal, M. R. SPE ANTEC Tech Paper 1997, 43, 2687.
19. Kamal, M. R.; Garmabi, H. S.; Arghyris, L. Polym Eng Sci 1995, 35, 41.
20. Wu, W.; Wagner, M. H.; Qian, Q.; Pu, W. G.; Kheirandish, S. J Appl Polym Sci 2006, 101, 2309.
21. Yeh, J. T.; Jyan, C. F. Polym Eng Sci 1998, 38, 1482.
22. Min, K.; White, J. L. Polym Eng Sci 1984, 24, 1327.
23. Jang, J. S.; Lee, D. K. Polymer 2004, 45, 1599.
24. Lee, S. Y.; Kin, S. C. Polym Eng Sci 1997, 37, 463.
25. Karami, A. K.; Balke, S. T. Polym Eng Sci 2000, 40, 2342.
26. Coleman, M. M.; Yang, X.; Zhang, H.; Painter, P. C. J Macromol Sci Phys 1993, 32, 295.
27. Venkatesh, G. M.; Gilbert, R. D.; Fornes, R. E. Polymer 1985, 26, 45.
28. Nir, Y.; Narkis, M.; Siegmann, A. Polym Eng Sci 1998, 38, 1890.
29. Ahn, T. O.; Kim, C. K.; Kim, B. K.; Jeong, H. M.; Huh, J. D. Polym Eng Sci 1990, 30, 341.
30. Petris, S.; De, P.; Malinconico, M.; Pracella, M. J Appl Polym Sci 1998, 68, 637.
31. Ka, C. S.; Ko, M. G.; Cho, W. J. Polymer 1997, 38, 1243.
32. Ding, Z. Y.; Hu, G. S.; Wang, B. B. J Polym Res 2007, 14, 511.
33. Wang, B. B.; Ding, Z. Y.; Hu, G. S. Polym Eng Sci 2008, 48, 2354.
34. Cebe, P.; Hong, S. D. Polymer 1986, 27, 1183.
35. Avrami, M. J. Chem Phys 1939, 7, 1103.
36. Avrami, M. J. Chem Phys 1940, 8, 212.
37. Jeziorny, A. Polymer 1978, 19, 1142.
38. Liu, T. X.; Mo, Z. S.; Wang, S.; Zhang, H. F. Polym Eng Sci 1997, 37, 568.
39. Ozawa, T. Polymer 1971, 12, 150.